J Solid State Electrochem (2009) 13:609–617
DOI 10.1007/s10008-008-0698-9

ORIGINAL PAPER

Growth and characterisation of diffusion junctions between paired gold electrodes: diffusion effects in generator–collector mode

Robert W. French · Frank Marken

Received: 19 August 2008 / Revised: 26 September 2008 / Accepted: 29 September 2008 / Published online: 25 October 2008

Abstract A diffusion junction between two paired gold electrodes is created in a bipotentiostatic electro-deposition process. Gold metal is deposited simultaneously on two adjacent disc electrodes (100 μm diameter, approximately 125 μm separation) until short-circuit conditions trigger the end point of the electro-deposition. Symmetric gold junctions with typically 5 μm average inter-electrode gap size, 140 μm gap length, and approximately 18 μm junction depth are obtained. These paired gold electrodes are employed in generator–collector mode to give well-defined steady-state feedback currents even for extremely low concentrations of analyte (sub-μM) and without any contributions from capacitive charging. Four redox systems are investigated spanning a wide range of diffusion coefficients: (1) the one-electron oxidation of iodide to iodine, (2) the two-electron oxidation of hydroquinone to benzoquinone, (3) the two-electron reduction of alizarin red S, and (4) the one-electron oxidation of the redox protein cytochrome *c*. Consistent results for these redox systems suggest that (1) the junction zone between the two electrodes is dominating the behaviour of the electrode in particular for the slower diffusing systems and (2) the paired gold electrode junction can be calibrated and employed for electroanalysis at very low concentrations and for a wider range of analytically relevant redox systems.

Keywords Nano-gap junctions · Microelectrode · Voltammetry · Generator–collector system · Gold electrode · Sensor · Hydroquinone · Iodide · Alizarin · Cytochrome *c*

Introduction

Micro-array and gap electrodes [1] offer, similar to ultra-microelectrodes [2], fundamentally interesting and practically powerful tools in electroanalytical chemistry. In contrast to ultra-microelectrodes, which are now widely commercially available and employed in routine electroanalytical measurements, simple micro-array and gap electrodes are difficult to obtain and, therefore, not commonly employed. Complex lithographic processes (e.g. for interdigitated array electrodes [3]) or sensitive micro-positioner devices can be employed in experiments where generator–collector diffusion junction systems are required, but these techniques are not very practical in everyday electroanalysis. We, therefore, attempted to directly grow metallic junctions by bipotentiostat-controlled electro-deposition. Over the recent years, several reports appeared where electro-deposition techniques have been developed for the formation of nanometer [4, 5] or even molecular-scale junctions [6–9]. The change in the 'cross-current' between two adjacent electrodes during the bipotentiostatic electrochemical growth process can be exploited as a reproducible measure of the gap size, and by stopping the electro-deposition process at a pre-defined cut-off current, well-defined junction geometries are obtained. This methodology is reproducible, and it does not require complex lithography nor micro-positioning processes.

The paired electrode junctions are most usefully employed in voltammetric experiments in feedback mode. Fast diffusion processes within this junction are driven by

Dedicated to Professor Keith B. Oldham, on the occasion of his 80th birthday

R. W. French · F. Marken (✉)
Department of Chemistry, University of Bath,
Claverton Down,
Bath BA2 7AY, UK
e-mail: F.Marken@bath.ac.uk

opposite potentials applied to the generator and collector terminals of the junction. Diffusion processes at similar paired microelectrode systems have been investigated and treated theoretically by Oldham [10], Stone [11], Svir [12] and Baur [13], usually for the case of paired inlaid discs or bands and for the case of paired hemisphere electrodes [14].

Generator–collector experiments are commonly carried out with micro-ring disc [15], rotating [16], or sono-ring-disc electrode systems [17], hydrodynamic double channel electrodes [18], SECM systems [19, 20], dual or array band [21] or interdigitated array electrodes [22]. Only for the latter two of these types of electrode systems can a symmetric diffusion field be established. The gap size for dual band or for interdigitated array electrode systems is crucial in determining the magnitude of the feedback current as well as the analytical sensitivity. Smaller gaps enhance the feedback current and are, therefore, more desirable. For lithographically produced electrode systems, the gap size is typically 10 to 100 μm. In the present work, paired gold electrodes are grown with a gap size of typically 5 μm.

The average gap size δ between generator and collector defines the time for the diffusion process to occur and, therefore, the limiting current $I_{\mathrm{lim}} = \frac{nFDAc}{\delta}$ (with n, the number of electrons transferred per molecule diffusing to the electrode; F, the Faraday constant; D, the average diffusion coefficient; A, the active electrode area and c, the concentration of the redox active species). For a pair of approximately hemispherical electrodes, the average gap size is not well defined, and rather distinct zones are present.

A schematic drawing in Fig. 1 illustrates paired electrodes with zones of fast, intermediate and slow diffusion, which also correspond to kinetic zones where fast, intermediate or slow reactions can be investigated. For redox systems with a sufficiently fast standard heterogeneous electron transfer rate constant $k_0 \geq D/\delta$, overall reversible electron transfer

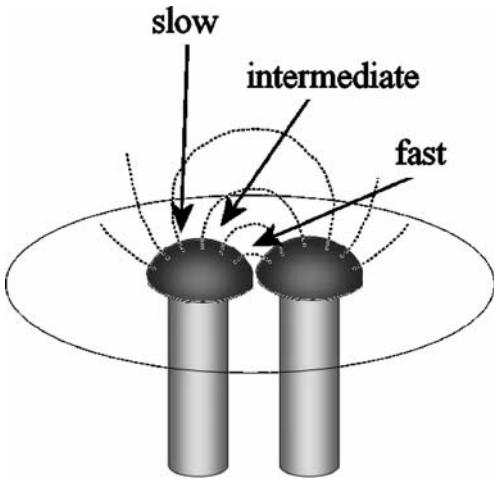

Fig. 1 Schematic drawing of two approximately hemispherical electrodes, the diffusion field and the kinetic zones reflecting *fast*, *intermediate* and *slow* transport processes

conditions are anticipated, and the currents flowing in the "fast zone" should dominate the overall process. We have recently demonstrated that paired gold electrodes with small inter-electrode gap may be used for nitric oxide electroanalysis [23]. In this report, a set of four redox systems is chosen to demonstrate that the ratio of the current flowing in the fast junction zone versus the overall current (e.g. the collection efficiency) can depend on the diffusion coefficient of the redox system.

Four redox systems are investigated (I^-/I_2, hydroquinone/benzoquinone, alizarin red S/hydroalizarin and ferri/ferro-cytochrome *c*) with sufficiently fast rate for effects from heterogeneous electron transfer to remain insignificant. Reversible electron transfer and fast diffusion within the gold junction are shown to produce highly sensitive collector currents without contributions from capacitive or other background currents. This allows analytically useful steady state voltammograms to be recorded down to sub-micromolar concentrations. The effects of the diffusion coefficient are considered and the potential for future analytical and electroanalytical applications discussed.

Experimental

Reagents

Chemical reagents such as potassium hydroxide, potassium gold(I)dicyanide, potassium cyanide, potassium dihydrogen phosphate, dipotassium hydrogen phosphate, potassium carbonate, poly-(diallyldimehtylammonium chloride) or PDDAC, potassium chloride, potassium iodide, H_2SO_4, hydroquinone, 4,4′-bipyridyl disulfide or aldrithiol-4 and alizarin red S were obtained commercially (Sigma–Aldrich) in analytical grade purity and used without further purification. Cytochrome *c* (equine heart, C7752, Sigma, 12384 Dalton) was purified by column chromatography using a PD-10 desalting column (Amersham Biosciences). Demineralised and filtered water was taken from a Vivendi purification unit with not less than 18 MOhm cm resistivity. Pureshield argon (BOC) was employed to de-aerate solutions. Experiments were conducted at 20±2 °C.

Instrumentation

For electrochemical and conductivity measurements a PSTAT30 biopotentiostat system (Autolab, EcoChemie, The Netherlands) was employed. In electrochemical experiments, a conventional three-electrode cell with platinum counter and saturated calomel reference (SCE, Radiometer, Copenhagen) were employed. Scanning electron microscopy (SEM) images were obtained using a JEOL JSM6480LV system. Samples were gold sputter-coated prior to SEM imaging.

Formation of paired gold electrode junctions

Platinum wires (100 μm diameter, approximately 10 cm long) were fed into two capillary glass tubes and then placed into a 5-mm outer diameter glass tube (approximately 8 cm long). This assembly was then heat-sealed at one end, and by carefully twisting, the two platinum wires were brought into close proximity. After cooling down, cutting and polishing, the two platinum disc electrodes are obtained with approximately 125 μm separation.

The bipotentiostatic electro-deposition cell was based on two working electrodes attached to the two platinum disc electrodes, a gold wire counter electrode and a SCE reference electrode. The plating solution was based on an alkaline cyanide bath (120 mg $KAu(CN)_2$, 200 mg KCN, 200 mg K_2HPO_4, 200 mg K_2CO_3 in 10 mL water (taken from reference [24]). Into this plating solution, 60 μL of 0.35 wt.% PDDAC was added to suppress dendritic crystalline gold growth. During deposition, the gold deposition bath was held at a constant temperature of 55 °C with continuous agitation.

Bipotentiostatic growth was carried out in a one-step process using the chronoamperometric method (GPES). Under the plating conditions, the reversible potential for the gold deposition process is approximately −0.86 V vs. SCE (obtained by cyclic voltammetry). One platinum disc electrode was set to a potential of −1.10 V vs. SCE for slow gold growth. The secondary platinum disc electrode was set to a slightly more negative deposition potential of −1.11 V vs. SCE. The difference in deposition potential was chosen small to minimise differences in the appearance of the resulting gold deposits. The automatic cut-off function (in the GPES software) was then used to stop the gold deposition process when the current exceeded 90 μA. The reason for the increase in deposition current close to the cut-off point is the onset of a short-circuit current between the two working electrodes in close proximity. After the cut-off point was reached, the electrode was removed from the gold plating bath, rinsed with demineralised water, dried and tested. Conductivity tests with the dry paired gold electrode junction revealed no direct short circuit or tunnel currents. Figure 2 shows typical SEM images of the paired gold electrode system. The position of the underlying platinum disc electrodes is indicated with a dashed line.

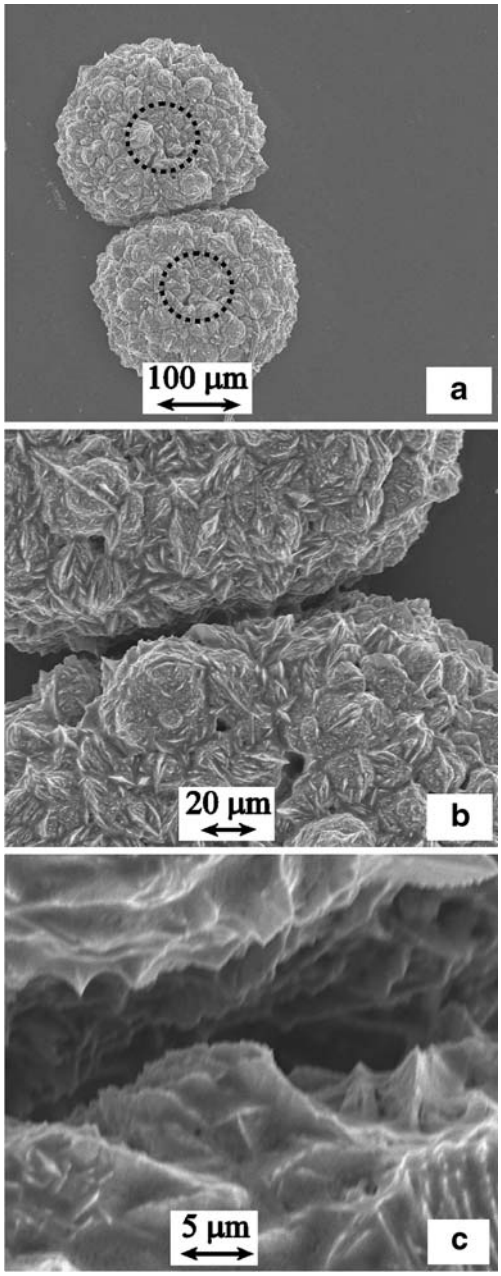

Fig. 2 Scanning electron micrograph (SEM) images of paired gold junction electrodes. **a** Low magnification view of the two gold deposits and indicated with a *dashed line* the approximate location of the underlying platinum disc electrodes. Higher magnification images are shown in **b** and in **c** and show a junction with approximately δ= 5 μm average gap

Results and discussion

Voltammetric characterisation of paired gold electrode junctions I.: oxidation of iodide

The oxidation of iodide in aqueous 0.125 M H_2SO_4 occurs as an overall one-electron mechanism (see Eq. 1 [25]). For this process, intermediates such as the I_3^- ion have been observed, but at sufficiently positive applied potential, a full conversion to I_2 is expected (see Eq. 1). This process is employed here as a model case for relatively fast diffusion (with $D_{\text{iodide}}=1.9\times10^{-9}$ m^2 s^{-1} [26, 27]).

$$I^- \rightleftarrows {}^1/_2\, I_2 + e^- \quad (1)$$

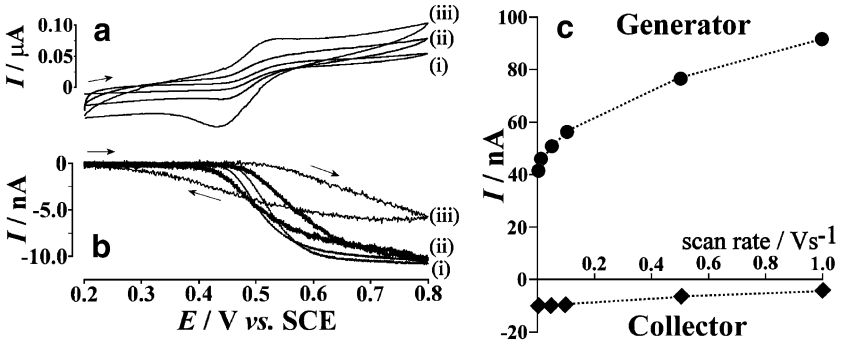

Fig. 3 **a** Cyclic voltammograms (scan rate *i* 5, *ii* 50, *iii* 500 mV s^{-1}) for the oxidation of 0.2 mM I^- in aqueous 0.125 M H_2SO_4 at a paired gold junction electrode with the collector held at a potential of 0.2 V vs. SCE. The generator current is shown. **b** The collector current is shown. **c** Plot of the peak or limiting currents observed for the generator and the collector electrode versus scan rate

Figure 3a shows typical voltammetric responses for the oxidation of 0.2 mM iodide in aqueous 0.125 M H_2SO_4. The generator electrode current plot shows a peak-shaped reversible response centered at 0.47 V vs. SCE at a scan rate of 0.5 V s^{-1} and a more step-shaped response at slower scan rate. The capacitive background current can be seen to dominate the voltammetric response. In contrast, the collector current (see Fig. 3b), which is recorded at a fixed potential of 0.2 V vs. SCE, shows a step-shaped steady-state response centered at approximately 0.52 V vs. SCE without any capacitive background current contributions. A clear diffusion-related hysteresis effect is observed to cause a mismatch of forward and backward scan. With increasing scan rate this hysteresis effect also increases. Dimensional analysis allows the average junction gap to be expressed as $\delta = \sqrt{\frac{DRT}{v_{\text{trans}}F}}$ (with D, the diffusion coefficient; R, the gas constant; T, the absolute temperature; F, the Faraday constant and v_{trans}, the scan rate where 'decoupling' of generator and collector occurs). With an average junction gap of $\delta \approx 5$ μm (see Fig. 2), the value for v_{trans} is approximately 2 V s^{-1} in approximate agreement with the data in Fig. 3b, where significant 'decoupling' is observed at a scan rate of 0.5 V s^{-1}. The steady-state limiting collector current can be obtained reliably up to a scan rate of 100 mV s^{-1} (see Fig. 3c). For the iodide or iodine redox system, additional effects may arise from unequal diffusion coefficients ($D_{\text{iodide}} \neq D_{\text{iodine}}$), and kinetic information about the formation of the tri-iodide intermediate (both beyond the scope of this report) may be contained in the fast scan rate collector current responses.

Next, the voltammetric response is recorded at a constant scan rate of 5 mV s^{-1} and for a range of iodide concentrations (see Fig. 4). Well-defined voltammetric responses are observed at the collector electrode even for sub-micromolar concentrations and good linearity of the plot of limiting current versus iodide concentration is observed over a range of 200 to 0.2 μM (see Fig. 4c). The estimated collection efficiency for the iodide/iodine redox system is approximately 30%.

Voltammetric characterisation of paired gold electrode junctions II: oxidation of hydroquinone

The oxidation of hydroquinone to benzoquinone is a well-known model redox process with similarity to many naturally occurring quinone or quinol redox processes [28]. In aqueous media, the process occurs as a chemically reversible two-electron oxidation (see Eq. 2) with short-lived semiquinone intermediates [29].

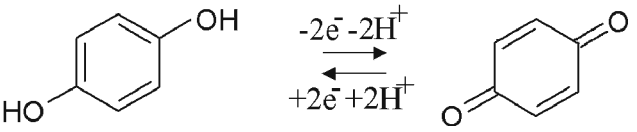

(2)

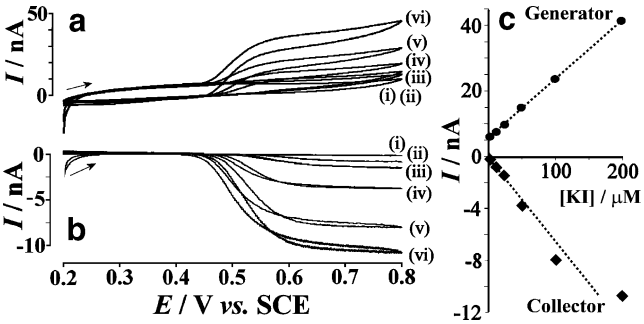

Fig. 4 **a** Cyclic voltammograms (scan rate 5 mV s^{-1}) for the oxidation *i* 1, *ii* 12, *iii* 25, *iv* 50, *v* 100 and *vi* 200 μM I^- in aqueous 0.125 M H_2SO_4 at a paired gold junction electrode with the collector held at a potential of 0.2 V vs. SCE. The generator current is shown. **b** The collector current is shown. **c** Plot of the limiting currents observed for the generator and the collector electrode versus iodide concentration

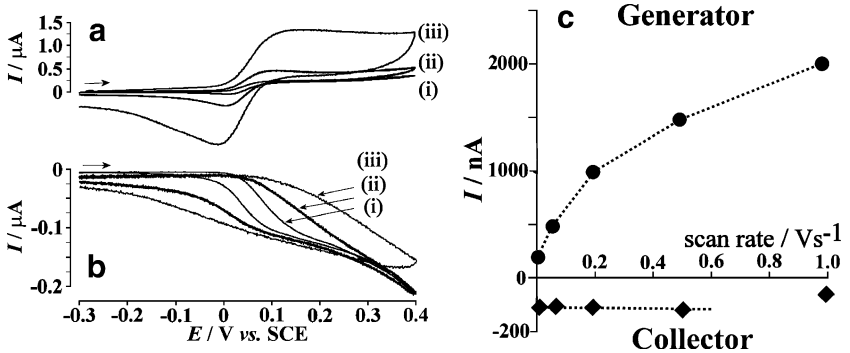

Fig. 5 **a** Cyclic voltammograms (scan rate *i* 5, *ii* 50, *iii* 500 mV s^{-1}) for the oxidation of 1 mM hydroquinone in aqueous 0.1 M phosphate buffer pH 7 at a paired gold junction electrode with the collector held at a potential of −0.3 V vs. SCE. The generator current is shown. **b** The collector current is shown. **c** Plot of the peak or limiting currents observed for the generator and the collector electrode versus scan rate

Figure 5 shows voltammetric data for the oxidation of 1 mM hydroquinone in aqueous 0.1 M phosphate buffer pH 7. Both generator and collector electrodes give well-defined current responses, although the limiting current at the collector electrode is virtually constant over a range of scan rates (see Fig. 5c). The hysteresis effect for the collector current is again observed (vide supra), but the effect is reduced (when compared to that for iodide oxidation). The decrease in hysteresis effect appears to be linked to the slower diffusion coefficient for hydroquinone ($D_{\text{hydroquinone}} = 0.85\times10^{-9}$ m^2 s^{-1} [27]). It is likely that processes for redox systems with a smaller diffusion coefficient are more dominated by gap-diffusion and, therefore, more confined in the junction gap with reduced hysteresis (vide infra). Due to the symmetry of the generator–collector electrode system, the diffusion coefficients for both hydroquinone and benzoquinone should be taken into account, but these are assumed here to be equal in first approximation.

The effect of the hydroquinone concentration on the voltammetric signal is shown in Fig. 6. The generator electrode response is non-linear which may be linked to effects of the electrode shape. However, the collector response is well defined and independent of the capacitive background and, therefore, more reliably measured especially in the low concentration range. The approximate collection efficiency can be estimated as 25%.

Voltammetric characterisation of paired gold electrode junctions III: reduction of alizarin red S

The alizarin red S redox system has been employed in adsorptive stripping voltammetry for example for boron [30], zirconium [31], for vanadium [32] or for copper [33, 34] and other oxophilic metals. The interaction of alizarin red S with proteins [35] and with DNA and damaged DNA [36] has been investigated by voltammetry. The mechanism

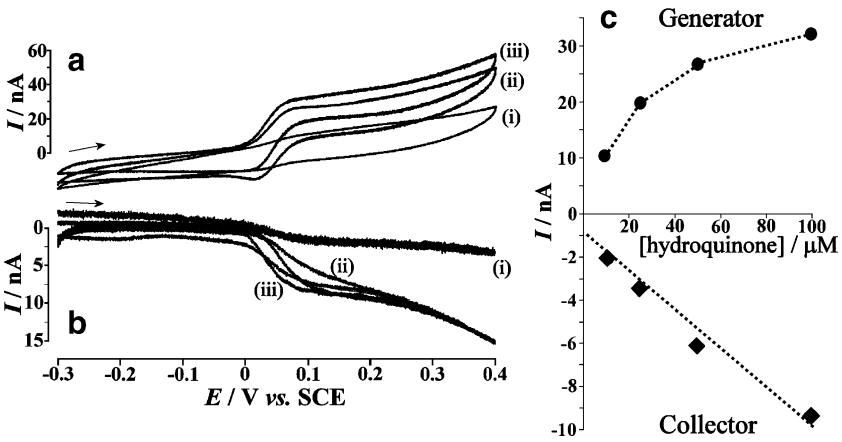

Fig. 6 **a** Cyclic voltammograms (scan rate 5 mV s^{-1}) for the oxidation of *i* 1, *ii* 10 and *iii* 100 μM hydroquinone in aqueous 0.1 M phosphate buffer pH 7 at a paired gold junction electrode with the collector held at a potential of −0.3 V vs. SCE. The generator current is shown. **b** The collector current is shown. **c** Plot of the peak or limiting currents observed for the generator and the collector electrode versus hydroquinone concentration

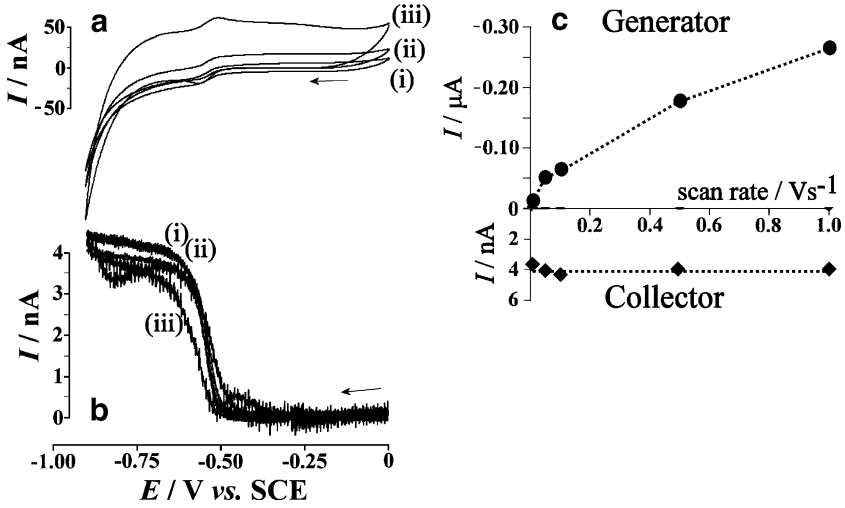

Fig. 7 **a** Cyclic voltammograms (scan rate *i* 5, *ii* 10, *iii* 100 mV s^{-1}) for the reduction of 0.2 mM alizarin S red in aqueous 0.1 M phosphate buffer pH 7 at a paired gold junction electrode with the collector held at a potential of −0.2 V vs. SCE. The generator current is shown. **b** The collector current is shown. **c** Plot of the peak or limiting currents observed for the generator and the collector electrode versus scan rate

for the reduction of alizarin red S follows a two-electron two-proton pathway [37, 38] (see Eq. 3).

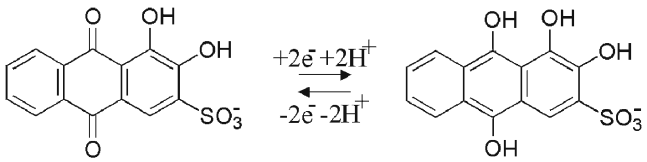

(3)

Figure 7 shows typical voltammetric responses for the reduction of 0.2 mM alizarin red S in aqueous 0.1 M phosphate buffer at pH 7. Both the reversible generator response and the collector signal are observed at ca. −0.55 V vs. SCE. The hysteresis effect is reduced (when compared to voltammograms for iodide and hydroquinone) and this may be attributed to a further reduced diffusion coefficient (with $D_{\text{alizarin}}=0.16\times10^{-9}$ m^2 s^{-1} [39], vide infra). Stable limiting currents are observed at the collector electrode even at scan rates up to 1 V s^{-1} (see Fig. 7c).

The effect of the alizarin red S concentration on the voltamemtric signals is summarised in Fig. 8. Well-defined collector responses are observed down to sub-micromolar concentrations. The collection efficiency can be estimated as ca. 18%.

Voltammetric characterisation of paired gold electrode junctions IV: reduction of cytochrome *c*

Finally, the Fe(III/II) cytochrome *c* redox system is investigated as an example of an extremely slow diffusion case. The diffusion coefficient for cytochrome *c* in aqueous phosphate buffer media has been reported as ca. 6×10^{-11} m^2 s^{-1} [40] consistent with an almost spherical protein of ca. 34 Å diameter. The cytochrome *c* redox system occurs naturally as an aqueous one-electron redox shuttle connecting cyto-

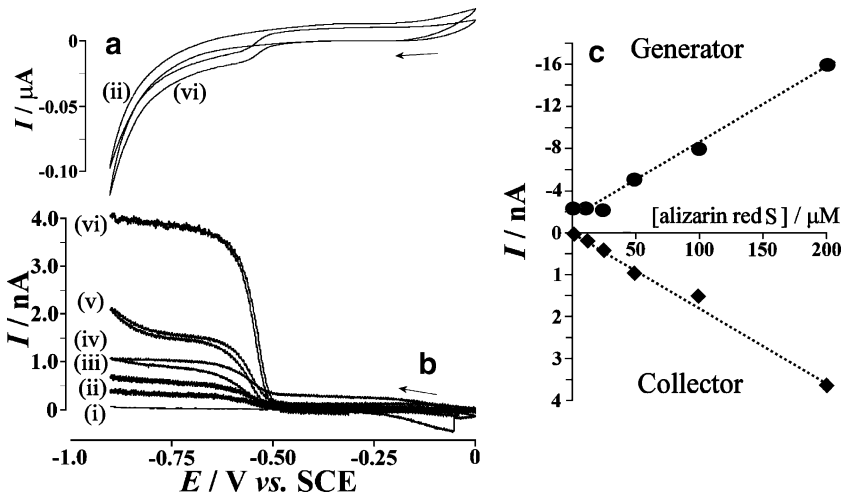

Fig. 8 **a** Cyclic voltammograms (scan rate 5 mV s^{-1}) for the reduction of *i* 1, *ii* 12.5, *iii* 25, *iv* 50, *v* 100 and *vi* 200 µM alizarin S red in aqueous 0.1 M phosphate buffer pH 7 at a paired gold junction electrode with the collector held at a potential of −0.2 V vs. SCE. The generator current is shown. **b** The collector current is shown. **c** Plot of the peak or limiting currents observed for the generator and the collector electrode versus hydroquinone concentration

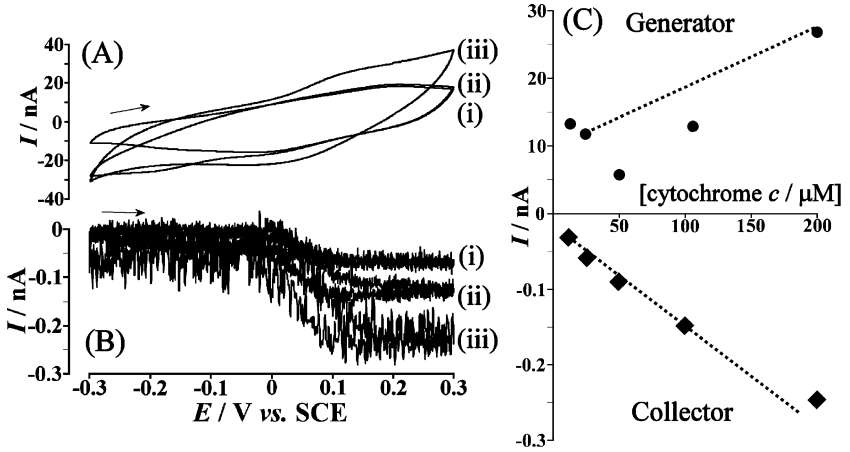

Fig. 9 **a** Cyclic voltammograms (scan rate 5 mV s^{-1}) for the reduction of *i* 25, *ii* 100 and *iii* 200 μM cytochrome *c* in aqueous 0.1 M phosphate buffer pH 7 at a paired gold junction electrode (gold surfaces modified by immersion into a solution of 1 mM 4,4′-bipyridyl disulfide or aldrithiol-4 in 0.1 M phosphate buffer pH 7) with the collector held at the open circuit potential observed prior to potential scan (typically 0.0 V vs. SCE). The generator current is shown. **b** The collector current (baseline corrected) is shown. **c** Plot of the peak or limiting currents observed for the generator and the collector electrode versus cytochrome *c* concentration

chrome oxidase and reductase in the respiration process [41]. Cytochrome *c* has been widely used as a model redox protein in electrochemistry [42] following the first observation of direct interfacial electron transfer at surface modified gold electrodes by Hill et al. [43]. The reagent 4,4′-bipyridyl disulfide, when adsorbed onto the gold electrode (from a 1 mM solution in 0.1 M phosphate buffer pH 7) prior to contact with cytochrome *c*, is effective in preventing interfacial protein denaturation and it provides a suitable "docking site" for the protein to effectively exchange electrons with the underlying gold surface. This approach is employed here to allow cytochrome *c* generator–collector experiments with two paired gold electrodes. The covalently attached heme unit within the cytochrome *c* molecule is responsible for a one-electron transfer (see Eq. 4 [44])

$$\text{Ferro} - \text{cytochrome } c \rightleftarrows \text{Ferri} - \text{cytochrome } c + e^- \qquad (4)$$

Cyclic voltammograms for the oxidation and re-reduction of 25, 100 and 200 μM cytochrome *c* dissolved in aqueous 0.1 M phosphate buffer pH 7 are shown in Fig. 9. Current responses at the generator and at the collector electrode were observed with a midpoint potential of approximately 0.05 V vs. SCE which is in good agreement with the literature value for the cytochrome *c* Fe(III/II) redox system [45]. The responses at the generator electrode are difficult to resolve in particular at lower concentrations of cytochrome *c*. In contrast, well-defined sigmoidally shaped current responses are observed at the collector electrode down to micro-molar concentrations of cytochrome *c* and only the increased background noise level at the pico-Ampère current range appears to limit the data quality. However, the clear collector current signals are obtained only after linear baseline correction which is necessary due to an additional drift current. It was possible to minimise the baseline current drift by starting the experiment at open-circuit conditions. The additional background current component may be due to adsorption of cytochrome *c* and/or due to conduction through a mono-layer of cytochrome *c* bound onto the glass surface within the junction.

The approximate collection efficiency for cytochrome *c* (estimated from Fig. 9c) is reduced to ca. 1.5%. For all redox systems studied in this report the magnitude of the collection efficiency appears to be strongly linked to the diffusion coefficient (see the plot in Fig. 10b). The reason for this correlation may be based on the spatial distribution of the feedback current (see Fig. 1). For a fast diffusing redox system, the process within the inter-electrode gap as well as considerable parts of the process outside of the gap contribute to the feedback current. In contrast, for a redox system with a very slow rate of diffusion, the inter-gap diffusion appears to dominate the feedback current. This causes a much lower overall collection efficiency. Both, the

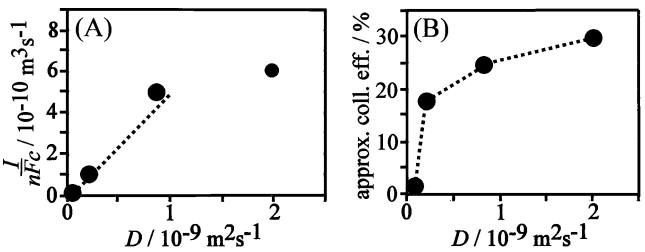

Fig. 10 **a** Plot of the concentration-normalised limiting current for the collector electrode (see Figs. 4c, 6c, 8c and 9c) versus the diffusion coefficients for cytochrome *c*, alizarin red S, hydroquinone and iodide (see text). **b** Plot of the approximate collection efficiency versus the diffusion coefficient

collection efficiency and the considerable hysteresis effect observed most clearly for iodide can be explained based on the same diffusion phenomenon.

Figure 10a shows a plot of the slopes of individual current versus concentration plots (see Figs. 4c, 6c, 8c and 9c) divided by nF versus the diffusion coefficient. For an electrode system dominated by gap diffusion a straight line plot is expected with a slope $\frac{I/nFc}{D} = \frac{A}{\delta}$. It can be seen that for systems with fast rate of diffusion such as iodide, the apparent slope $\frac{A}{\delta}$ is too low and, therefore, δ is too high. For this system diffusion outside of the inter-electrode junction is significantly contributing to the current. If only the data points for the redox systems with lower rate of diffusion are considered, the slope can be estimated as $\frac{A}{\delta} = \frac{h \times l}{\delta} \approx 0.5$. The average gap size δ=5 μm and the gap length l=140 μm can be obtained from the SEM shown in Fig. 2. Therefore the approximate junction height is determined as ca. h= 18 μm.

Conclusions

It has been shown that paired gold electrode junctions can be grown bipotentiostatically by controlled gold electrodeposition. A short-circuit current cut-off trigger mechanism allows junctions to be formed reproducibly and with an average gap size of approximately 5 μm. The paired junction electrode system has been characterised with four redox systems selected to provide data for a wide range of diffusion coefficients. For all four redox systems, measurements at very low concentrations were feasible due to the extremely low background currents observed for the steady state collector currents. Data analysis shows that for redox systems with sufficiently low diffusion coefficients, gap diffusion dominates and the gap dimensions can be estimated. In future, this type of paired electrode system will be useful in analytical measurements at very low concentration levels and for short lived intermediates. Work on further narrowing the gap between the paired electrodes in order to increase sensitivity and speed is in progress.

Acknowledgements R.W.F. thanks the Innovative Electronic Manufacturing Research Council (IeMRC) for a studentship ("Molecular Junctions—Made to Measure").

References

1. Amatore C (1995) In: Rubinstein I (ed) Physical electrochemistry. Marcel Dekker, New York, p 131
2. Ordeig O, del Campo J, Munoz FX, Banks CE, Compton RG (2007) Electroanalysis 19:1973. doi:10.1002/elan.200703914
3. Tomcik P, Jursa S, Bustin D, Tvarozek V (1998) Chemicke Listy 92:626
4. Carrara S, Riley DJ, Bavastrello V, Stura E, Nicolini C (2005) Sens Actuators B Chem 105:542. doi:10.1016/j.snb.2004.06.020
5. Li CZ, He HX, Tao NJ (2000) Appl Phys Lett 77:3995. doi:10.1063/1.1332406
6. Chen F, Tao NJ (2007) In: Staikov G (ed) Electrocrystallization in Nanotechnology. Wiley, Weinheim, p 167
7. Chen F, Quing Q, Ren L, Wu Z, Liu Z (2005) Appl Phys Lett 86:123105. doi:10.1063/1.1871361
8. Qing Q, Chen F, Li PG, Tang WH, Wu ZY, Liu ZF (2005) Angew Chem Int Ed 44:7771. doi:10.1002/anie.200502680
9. Deshmukh MM, Prieto AL, Gu Q, Park H (2003) Nano Lett 3:1383. doi:10.1021/nl034538p
10. Oldham KB (1992) J Electroanal Chem 323:53. doi:10.1016/0022-0728(92)80003-M
11. Phillips CG, Stone HA (1997) J Electroanal Chem 437:157. doi:10.1016/S0022-0728(97)00395-1
12. Svir IB, Oleinick AI, Compton RG (2003) J Electroanal Chem 560:117. doi:10.1016/j.jelechem.2003.07.023
13. Baur JE, Motsegoog PN (2004) J Electroanal Chem 572:29. doi:10.1016/j.jelechem.2004.05.022
14. Alfred LCR, Oldham KB (1995) J Electroanal Chem 396:257. doi:10.1016/0022-0728(95)04067-X
15. Harvey SLR, Parker KH, O'Hare D (2007) J Electroanal Chem 610:122. doi:10.1016/j.jelechem.2007.07.006
16. Pleskov YV, Filinovskii VY (1976) The rotating disc electrode. Plenum, New York
17. Nei LB, Marken F, Hong Q, Compton RG (1997) J Electrochem Soc 144:3019. doi:10.1149/1.1837953
18. Thompson M, Klymenko EV, Compton RG (2005) J Electroanal Chem 576:333. doi:10.1016/j.jelechem.2004.10.029
19. Nagy G, Nagy L (2000) Fresenius J Anal Chem 366:735. doi:10.1007/s002160051567
20. Liljeroth P, Johans C, Slevin CJ, Quinn BM, Kontturi K (2002) Anal Chem 74:1972. doi:10.1021/ac015720i
21. Streeter I, Fietkau N, Del Campo J, Mas R, Munoz FX, Compton RG (2007) J Phys Chem C 111:12058. doi:10.1021/jp073224d
22. Aoki K (1993) Electroanalysis 5:627. doi:10.1002/elan.1140050802
23. French RW, Collins AM, Marken F (2008) Electroanalysis. doi:10.1002/elan.200804354
24. Schlesinger M, Paunovic M (2000) Modern electroplating. Wiley, New York, p 205
25. Akkermans RP, Qiu FL, Roberts SL, Suarez MF, Compton RG (1999) J Phys Chem B 103:8319. doi:10.1021/jp991778d
26. Marken F, Akkermans RP, Compton RG (1996) J Electroanal Chem 415:55. doi:10.1016/S0022-0728(96)04641-4
27. Adams RN (1969) Electrochemistry at solid electrodes. Marcel Dekker, New York, p 220
28. Nurmi JT, Tratnyek PG (2002) Environ Sci Technol 36:617. doi:10.1021/es0110731
29. Bauscher M, Mantele W (1992) J Phys Chem 96:11101. doi:10.1021/j100205a087
30. Sahin I, Nakiboglu N (2006) Anal Chim Acta 572:253. doi:10.1016/j.aca.2006.05.049
31. Li YH, Zhao QL, Huang MH (2007) Mikrochim Acta 157:245. doi:10.1007/s00604-006-0655-1
32. Li YH, Wang YX, Huang MH (2008) Electroanalysis 20:1440. doi:10.1002/elan.200804200
33. Shiu KK, Song FY (1998) Electroanalysis 10:256 doi:10.1002/(SICI)1521-4109(199804)10:4<256::AID-ELAN256>3.0.CO;2-K
34. Deng PH, Fei JJ, Zhang J, Li JN (2008) Electroanalysis 20:1215. doi:10.1002/elan.200704168
35. Sun W, Jiao K (2002) Talanta 56:1073. doi:10.1016/S0039-9140(01)00628-2
36. Yang ZS, Zhang DP, Long HY, Zhao GC (2007) Electroanalysis 19:2577. doi:10.1002/elan.200704016

37. Mouchrek VE, Marques ALB, Zhang JJ, Chierice GO (1999) Electroanalysis 11:1130 doi:10.1002/(SICI)1521-4109(199911)11:15<1130::AID-ELAN1130>3.0.CO;2-3
38. Mirceski V, Lovric M (1997) Electroanalysis 9:1283. doi:10.1002/elan.1140091613
39. Abdel-Hamid R, Rabia MK, El-Sagher HM (1997) Bull Chem Soc Jpn 70:2389. doi:10.1246/bcsj.70.2389
40. Hill HAO, Nakagawa Y, Marken F, Compton RG (1996) J Phys Chem 100:17395. doi:10.1021/jp961347k
41. Stryer L (1995) Biochemistry, 4th edn. Freeman, New York
42. McKenzie KJ, Marken F (2003) Langmuir 19:4327. doi:10.1021/la0267903
43. Eddowes MJ, Hill HAO (1979) J Am Chem Soc 101:4461. doi:10.1021/ja00510a003
44. Toth AB, Chambers JQ (2002) Electroanalytical methods for biological materials. Marcel Dekker, New York
45. Eddowes MJ, Hill HAO, Uosaki K (1979) J Am Chem Soc 101:7113. doi:10.1021/ja00517a077